

Performance Optimization of OSAJ P-Type Ga As IMPATT Diodes

EL-SAYED A. EL-BADAWY

SM IEEE, Member of OSA.

Dean, Head of ECE Department, Professor of Communication and Electronics,

Alexandria Higher Institute of Eng. & Technology (AIET),

Alexandria 21311, Alexandria, Egypt.

E-mail: sbadawy@ieee.org, dean@ait.edu.eg, sbadawy41@gmail.com

SAID H. IBRAHIM

Computer and Electronics Engineering Department.

King Faisal University

Al-Ahsa P.O. Box 400 Tel. 0096635800000

K.S.A.

saidhassan1@yahoo.com

Abstract: The study of OSAJ p-type Ga As IMPATT diode is important in order to get better insight into the operation of this type, which is not sufficiently studied. Hence it will be possible to design and optimize the structure of double-drift Ga As IMPATT and the circuit where this IMPATT is embedded. This paper presents the results of detailed study for performance optimization of OSAJ p-Type Ga As IMPATT Diode structures. This study used the full-scale computer simulation program performed by the authors taking into consideration the nonlinearities and all physical effects pertinent to the IMPATT operation. Some important conclusions concerning the effect of the peak value of the microwave signal, the effects of the operating dc-bias current and the operating frequency on the IMPATT operation and performance are drawn. The complete simulation curves for the operation of OSAJ p-type IMPATT diodes are introduced

Key Words: Microwave Circuit Design, Microwave Devices, Computer Aided Design

1 Introduction

The optimization of one-sided abrupt junction (OSAJ) P-type Ga As IMPATT diode is very difficult due to the complexity of transport equations governing its operation and sever nonlinearities inherent them. The matter is complicated further by relatively large number of structural parameters, which have to be optimized simultaneously by taking into account that they affect the performance in a competitive direction [1-9].

This paper shed further light on the effect of peak RF Voltage, DC bias current, and the operating frequency on the performance of OSAJ P-Type Ga As IMPATT diodes. This is to help the designer to optimize the performance of these diodes.

This paper presents the results of a detailed study of p-type Ga As IMPATT [10-15]. These results are obtained using a modified version of the full-scale computer-simulation program

performed by the authors [1-5, 16,17]. This program takes fully into account the nonlinearities and all the physical effects pertinent to the IMPATT operation.

The system of the continuity equations are presented below in a normalized form[16]:

$$\frac{\partial n(x,t)}{\partial t} = \frac{\partial J_n(x,t)}{\partial x} + \alpha_n |J_n(x,t)| + \alpha_p |J_p(x,t)| \quad [1]$$

$$\frac{\partial p(x,t)}{\partial t} = \frac{\partial J_p(x,t)}{\partial x} + \alpha_n |J_n(x,t)| + \alpha_p |J_p(x,t)| \quad [2]$$

$$J_n(x,t) = n(x,t)V_n + D_n \frac{\partial n(x,t)}{\partial x} \quad [3]$$

$$J_p(x,t) = p(x,t)V_p - D_p \frac{\partial p(x,t)}{\partial x} \quad [4]$$

where n, p are the concentrations of electrons and holes; J_n, J_p are the spatial distribution of the electron and hole currents; α_n, α_p are the ionization coefficients; V_n, V_p are the drift velocities; D_n, D_p are the diffusion coefficients. Ionization coefficients, drift velocities and

diffusion coefficients are the functions of two arguments; the space coordinate x and the time t .

The electrical field distribution in semiconductor structure can be obtained from the Poisson equation and can be defined in the following normalized form [16]:

$$\frac{\partial E(x,t)}{\partial x} = -\frac{\partial^2 U(x,t)}{\partial x^2} = N_D(x) - N_A(x) + p(x,t) - n(x,t) [5]$$

where $N_D(x)$, $N_A(x)$ are the concentrations of donors and acceptors accordingly, $U(x,t)$ is the potential, $E(x,t)$ is the electrical field.

Whereas the performance of n-type Ga As IMPATT is extensively studied, the performance of the p-type one is not sufficiently studied [10-15]. This is attributed mainly to the superiority of the velocity-field characteristic of n-type Ga As IMPATT [10-12, 14,15]. However, the investigation of p-type IMPATT is necessary for the design and optimization of double-drift Ga As IMPATT and also for the optimum design of the microwave circuit where the IMPATT is embedded.

The results that will be presented are obtained for OSAJ P-type IMPATT diode structure whose width of the active region (w) is 3.3 μm , doping density in the ohmic contact p^+ and n^+ is $2 \times 10^{17} \text{ cm}^{-3}$ and doping density in the active region is $5 \times 10^{15} \text{ cm}^{-3}$. The ionization rates used in the simulation are those measured by Kao and Crowel [18-20].

The diode is assumed to be placed in a high-Q cavity supporting a sinusoidal signal of amplitude (P) and it is driven by a terminal voltage V_T whose dc component is V_{DC} and ac component is a sinusoidal voltage of peak P and frequency F .

2 Results

Figures 1 and 2 show the efficiency (η), the RF power (P_{RF}), the diode conductance (G_D), and the breakdown voltage (V_B) versus P .

Figure 1 indicates that there is an optimum value of P where η and P_{RF} have their maximum values. This optimum value is about 67V. Figure 2 shows that G_D and V_B are monotonically decreasing with P .

Figures 3 and 4 show the η and P_{RF} versus F for dc bias current (J_{dc}) ranging from

1000 to 4000 A/cm^2 . It is seen that the maximum efficiency is shifted toward higher frequencies as J_{dc} is increased. Namely the optimum frequency is 11 GHz at $J_{dc} = 500 \text{ A/cm}^2$ and 14.5 GHz at $J_{dc} = 4000 \text{ A/cm}^2$.

Figure 5 and 6 show η and P_{RF} versus P of the RF terminal voltage for J_{dc} ranging from 500 to 3500 A/cm^2 . It is noticed that the optimum peak increases slightly with J_{dc} . For example, the optimum peak is 61 V for $J_{dc} = 500 \text{ A/cm}^2$ against 64 V for $J_{dc} = 2500 \text{ A/cm}^2$. The dependence of P_{RF} and η on the J_{dc} for $P=50 \text{ V}$ and $F=11 \text{ GHz}$ is illustrated explicitly in figure 7. These results and the other results presented here will be interpreted physically in the next sections.

3 Analysis of the effect of the peak values of MW signal

In order to get a better insight into the previous results it is necessary to investigate the dynamics of the charge carriers within the diode and their interaction with the electric field (E). It is also necessary to study the resultant induced current waveforms for different values of P .

Figures 8 through 14 show the induced current (J_i), and the spatial distribution of the hole current (J_p) and the electric field (E) at different phase angles (Θ) during the RF cycle and for different values of P . By considering these figures, the large-signal operation of the p-type Ga As IMPATT can be explained as follows:

At the beginning of the cycle J_i decreases as the trailing edge of the avalanche-generated pulse (AGP) of holes of the previous cycle is being extracted at the right end of the drift region (DR). As P increases, this extraction becomes more efficient and J_i drops to smaller values. This helps improve the performance through reducing the effective saturation current and increasing the phase delay provided by the avalanche process. However, for the values of P higher than the optimum value, the AGP will drift at velocities smaller than the saturated velocity and the value of J_i at the beginning of the cycle increases again and the performance is degraded.

As the RF voltage increases during the positive half-cycle, E increases inside the diode and the avalanche generation causes J_i to increase. This increase becomes sharper as P increases. This is because the ionization rates are very sensitive to the field variation. It is seen that the hump of J_i becomes sharper and higher as P increases. This indicates that the AGP becomes more localized in both space and time when P is increased. This increased localization of AGP is attributed to the reduction of the saturation current, the reduction of space charge effect (SCE), and the reduction of the carrier generation in the DR. when P increased. The reduction of all these effects help to improve the performance and causes P_{RF} and η to increase initially with P .

The decrease of J_i after attaining its peak value is attributed to the extraction of the minority carriers (the electron) at the n^+ contact. The AGP of holes is injected into the DR and if P is small, this pulse is sufficiently wide that its extraction starts early causing J_i to decrease. As the AGP drifts in the DR, it is dispersed by the effect of the diffusion. If P is increased the E in the DR during the negative half-cycle becomes lower than the value necessary to saturate the electron velocity. This effect is known as drift-velocity dropping below saturation (DVDBS) and causes J_i to undergo a dip at phase angles around 270 degrees, i.e. at the worst time for the RF power generation. This effect becomes more pronounced as P increases and causes the performance to be degraded if P is excessively high. On the other hand, the carrier generation in the DR during the negative half-cycle becomes less significant as P increases. This improves the performance, since these carriers induce currents that are not in proper phase relationship with that induced by the AGP. When P is too large, the E at the right end of the DR may become negative and mobile holes will be injected into the DR inducing a current in an antiphase relationship with that of the AGP. This effect, which is known as the depletion-layer width modulation (DLWM) effect is responsible for the performance degradation as P increases.

4 EFFECT OF P ON G_D AND V_B

Its seen in figure 2 that the magnitude of the negative conductance decreases with P . This is because at constant dc current the avalanche pulse of fixed charge forces fixed amplitude for the fundamental of J_i . This means that as P increases, the induced current electronic conductance must decrease. The decrease of G_D with P assures a stable oscillator operation. It is also seen that V_B decreases with P . This effect is caused by the nonlinearity of the device and is explained as follows: As P increases, the E in the avalanche region attains higher values during the portion of the cycle at which the significant avalanche generation occurs. Hence, greater amount of charge carriers would be generated. Nevertheless, the total amount of charge is a constant imposed by the dc bias current. Hence, the dc component of the E and, correspondingly, the dc voltage should decrease as P is increased to maintain a constant current under breakdown conditions.

5 Analysis of the effects of the DC bias current

As J_{dc} is increased the number of carriers generated by the avalanche process and injected into DR increases. This effect is illustrated in figures 15 through 17. Figures 15 through 17 show J_p and E at $\Theta = 0, 90, 180,$ and 270 degree respectively for $F=11$ GHz and $P=60$ V at J_{dc} ranging from 500 to 5000 A/cm². It is seen that the size and the height of AGP increases with J_{dc} . This causes the hump of J_i occurring near $\Theta=180^\circ$ to increase with J_{dc} . This effect is illustrated in figure 18 that shows J_i and the terminal voltage (V_t) for different values of J_{dc} . This effect improves the performance since the number of carriers contributing to the power generation mechanism increases. Consequently, the P_{RF} increases with J_{dc} as figure 7 shows.

On the other hand, as J_{dc} is increased, the SCE becomes more pronounced. This effect causes E behind the AGP to increase and that in the front of it to decrease. This is shown in figures 15 through 17. The depression of the field behind the AGP reduces the phase delay provided by the avalanche process. This effect is the major factor responsible for the performance degradation as J_{dc} is increased.

The increase of E in the front of the AGP either reduces or totally suppresses the DVDBS effect and the depletion layer width modulation (DWM) effects. Consequently, the optimum value of P increases with J_{dc} . The DLWM effect is shown in figure 15. It is responsible for the dip occurring in J_i at $\Theta \cong 270^\circ$ as it is illustrated in figure 18. As J_{dc} is increased, this dip is removed because of the suppression of the DLWM. For higher values of J_{dc} , E will have a second peak that is moving in front of the AGP. This effect is shown in figures 16 and 17 and the minority carriers enhancement effect increases. Hence the performance is degraded.

As J_{dc} is excessively increased, the field behind the AGP is considerably reduced and some carriers will be trapped in the middle of the DR. This effect is illustrated in figures 16 and 17 and is also responsible for the performance degradation as J_{dc} is increased.

6 Analysis of the effects of frequency

For a give IMPATT structure and operating bias current there is an optimum frequency at which the total phase delay provided by the two mechanisms responsible for IMPATT operation is about 180° [10-15]. These two mechanisms are essentially the avalanche mechanism and the transit-time mechanism.

If the frequency is increased above its optimum value, the time available for the extraction of the AGP will be smaller and a higher number of carriers will still be existing in the DR during the last portion of the RF cycle. Consequently, J_i will be higher as F is increased during this portion. This effect is illustrated in figures 15, 18, 19, 20 and 21 which show J_i , J_p and E for $F=11, 7$ and 15 GHz respectively. The performance from this point of view is improved. However, the number of carriers still existing at the end of the cycle and at the beginning of the next cycle will increase with frequency. Hence the power dissipation will increase and the avalanche process will start earlier as F is increased. This will reduce the phase delay provided by the avalanche process and the performance will be degraded.

If the frequency is decreased below its optimum value, the carriers will be extracted early and J_i drops more rapidly during the negative half cycle. However, the time during which V_t exceeds the breakdown level increases. This allows the AGP to attain higher values. Consequently, J_i will attain a higher hump at $\Theta \cong 180^\circ$; figures 20 and 21; as F is increased. This effect improves the performance. The increase of the size of the AGP is attributed to the fact that a higher charge is required to maintain the bias current if F is increased; the SCE becomes more pronounced as F is decreased.

7 Conclusions

From the investigation of the large-signal results presented in this paper, the following conclusions concerning the effects of the RF voltage amplitude on the diode performance are drawn. As P is increased, the AGP of holes becomes shaper both in the time and in space. As P is increased, the SCE becomes less significant. Hence the phase delay provided by the avalanche generation process is increased and the performance is improved. As P is increased, J_i becomes generally lower in the positive half-cycle and higher in the negative half-cycle. This effect is explained by the previously mentioned effects. During the negative half-cycle, the carrier generation in the DR becomes less significant as P is increased. As P is increased, DVDBS becomes more significant, and the performance is degraded. As P is excessively increased, the DLWM will deteriorate the performance significantly.

Concerning the effects of the dc bias current on the P-type IMPATT the following conclusions are drawn:

As J_{dc} increases, the number of carriers that can contribute to the RF power generation increases. This improves the performance. On the other hand, the SCE increases with J_{dc} . This effect improves the performance through suppressing or at least reducing the DVDBS and the DLWM effects. In addition, the optimum value of the peak of the RF voltage increases. However, as the SCE becomes more pronounced, the phase delay caused by the avalanche process is reduced, the generation of the minority carriers in the DR is enhanced,

and the carrier trapping behind the AGP during the negative half cycle becomes more significant. All these effects cause the performance to be degraded as J_{dc} is increased.

The following conclusions concerning the effects of the operating frequency on the performance are drawn: For each IMPATT structure, there is an optimum frequency at which the total phase delay provided by the mechanism responsible for IMPATT operation is around 180° . For a higher frequency a greater number of carriers will be extracted at the beginning of the RF cycle. This increases the power dissipation and reduces the phase delay provided by the avalanche process. In addition, the AGP will be wider. All these effects degraded the performance. If the frequency is lower than the optimum one, the carriers will be extracted early and J_i decreases during the negative half cycle. This degrades the performance. Furthermore, the SCE becomes more pronounced as F is decreased.

References:

- [1] D.Christiansen, C.K.Alexander, and R.K. Jurgen (eds) " Standard handbook of Electronic Engineering (5th edition), McGraw Hill, 2006, ISBN 0-07-138421-9
- [2] P. Bauhahn and G. I. Haddad, "IMPATT device simulation and properties," IEEE Trans. Electron Devices, vol. ED-24, Jan., 1977.
- [3] Yuan, M. R. Melloch, J. A. Cooper, and K. J. Webb, "Silicon Carbide IMPATT Oscillators for High-Power Microwave and Millimeter-Wave Generation," IEEE/Cornell Conference on Advanced Concepts in High Speed Semiconductor Devices and Circuits, Ithaca, NY, August 7-9, 2000.
- [4] K. Mouthan, "Two frequency operation of the avalanche-transit-time oscillators," Proc. IEEE(Lett.), vol. 58, March, 1970.
- [5] W. E. Schroeder and G. I. Haddad, " Effect of harmonic and subharmonic signals on avalanche diode oscillator performance," IEEE Trans. Microwave Theory Tech., vol.MTT-18, June, 1970.
- [6] BJ H Zhao, V Gruzinskis, Y Luo, M Weiner, M Pan, P Shiktorov and E Starikov, "Monte Carlo simulation of 4H-SiC IMPATT diodes", 2000 Semicond. Sci. Technol. 15 1093-1100
- [7] S R Pattanaik et al , "Prospects of 6H-SiC for operation as an IMPATT diode at 140 GHz", 2005 Semicond. Sci. Technol. 20 299-
- [8] Robert E. Collin," Foundations of Microwave Engineering", McGraw-Hill, 1992.
- [9] J.Anaslassiades et al, " Solid-State Microwave Generators", Chapman & Hall, 1992.
- [10] El-Sayed A. El-Badawy, S.H. Ibrahim, and H. A. El-Motaafy," Effect of the Variation of the Doping Densities on the Performance of High Efficiency LHL In P IMPATT Diodes", 1997, IEEE AP-S International Symposium and URSI North American Radio Science Meeting, Montreal, Canada, July 15-18,1997
- [11] H. El-Motaafy , El-Sayed A. Badawy, and S.H Ibrahim, Al.,"Analysis of Low-High-Low InP IMPATT reflection amplifiers", ANTEM'98, Symposium on Antenna and applied electromagnetic, Aug. 1998, Ottawa, Ontario, Canada.
- [12] S.H. Ibrahim, El-Sayed A. El-Badawy, and H. A. El-Motaafy," Effect of the Operating Conditions on the performance of high Efficiency In P IMPATT Diodes," International Wireless Telecommunications Symposium / Exhibition, May 14-16, 1997 Shah Alam, Malaysia.
- [13] Binod K. Kanaujia, A. K. Singh, and B. R. Vishvakarma, , " IMPATT diode integrated annular ring microstrip antenna", Journal of Microwaves and Optoelectronics, Vol. 3, N.o 5, July 2004
- [14] Hosny A. El-Motaafy,"The optimum width of LHL IMPATT diodes,"Proceeding of the first Conference Aeronational Science and Aviation Tech., MTC., Cairo, Egypt, May, 1985.
- [15] H. A. El-Motaafy," The optimum voltage waveform for silicon IMPATT diodes," 7th Conference on Solide-State Science, cairo, 1984.
- [16] Alexander M. ZEMLOAK, Carlos CELAYA-BORGES, and Roque De La CRUZ," Nonlinear Analysis of Double Avalanche Region IMPATT Diode", IEICE TRANS. ELECTRON., VOL. E88-C, No. 1 January 2005.
- [17] H. El-Motaafy, " Full-scale computer simulation of TRAPATT diodes," " The Third National Radio-Science Symposium, Cairo, 1985.
- [18] C. W. Kao, and C. R. Crowel," Impact ionization by electron and holes in InP", Solid state electron, Vol. 23 pp 881-891, 1980.
- [19] S.H.Ibrahim, et-al," Analysis of the modes of operation of InP IMPATT diodes using C.

Kao and C. R. Crowel ionization rates”, Sixth National Radio Science Conference, Feb. 19-21, 1989.

[20] El-Motaafy, Al-Arabaty, and S.H. Ibrahim,” Effects of the Ionization Rates on the Large-Signal Performance of High Efficiency In P IMPATT Diodes”, Seventh National Radio Science Conference, Feb. 20-22, 1990, Cairo, Egypt

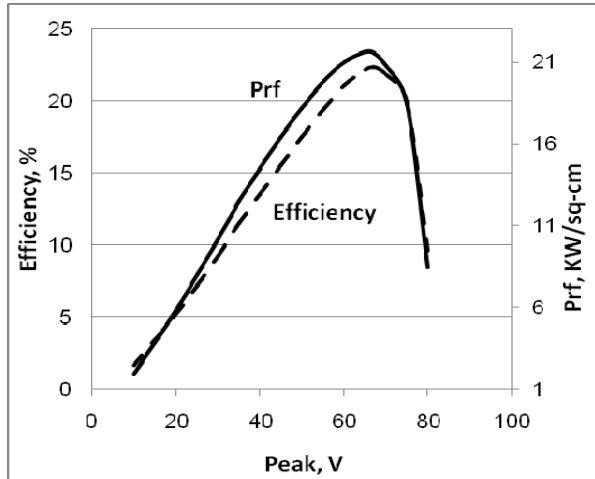


Fig. 1: The efficiency and RF power (Prf) versus the peak voltage

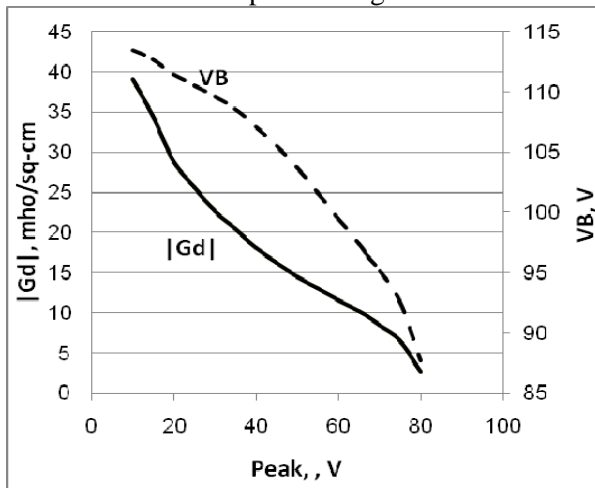


Fig. 2: The diode conductance ($|G_d|$) and breakdown voltage (V_B) versus the peak voltage

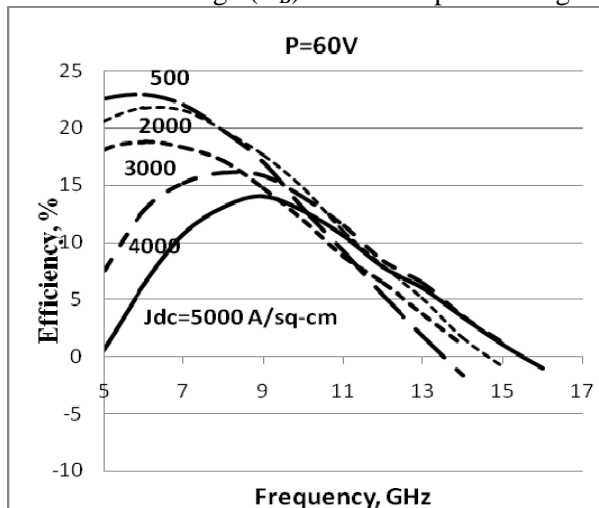


Fig. 3: The efficiency versus frequency for dc bias current (J_{dc}) ranging from 500 A/cm^2 to 4000 A/cm^2

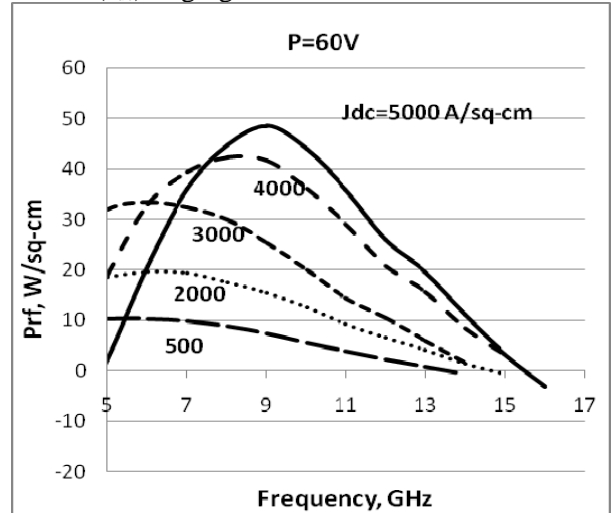


Fig. 4: The RF Power (P_{RF}) versus frequency for dc bias current (J_{dc}) ranging from 500 A/cm^2 to 4000 A/cm^2

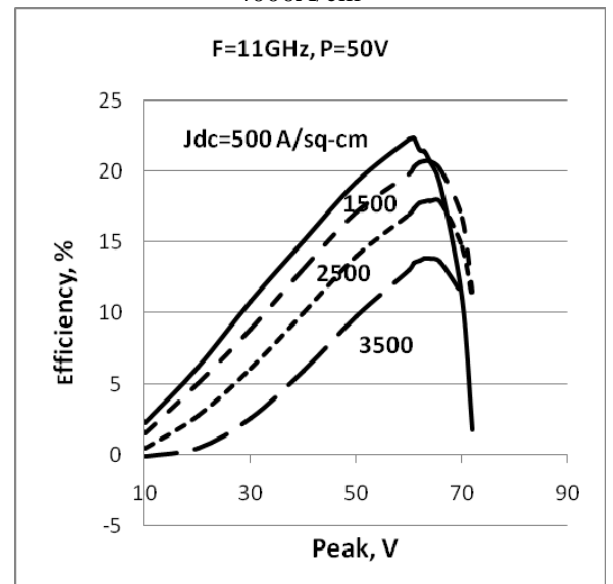


Fig. 5: The efficiency versus terminal voltage (V) for dc bias current ranging from 500 A/cm^2 to 3500 A/cm^2

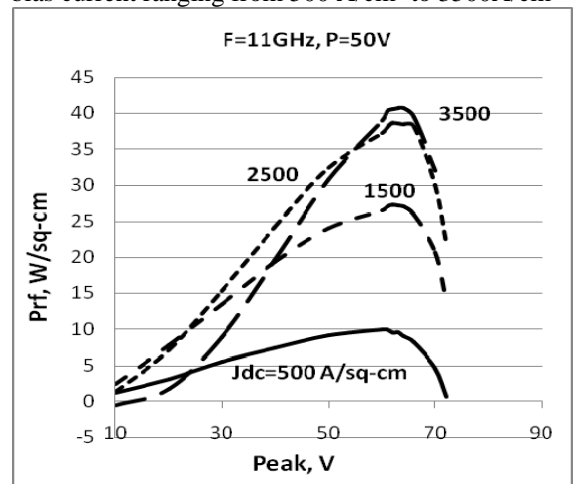


Fig. 6: The RF Power (P_{RF}) versus terminal voltage (V) for dc bias current (J_{dc}) ranging from 500 A/cm^2 to 3500 A/cm^2

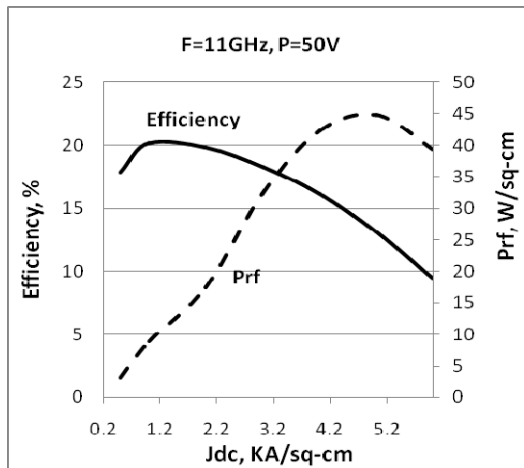


Fig. 7: The RF Power (Prf) and efficiency versus dc bias current (J_{dc})

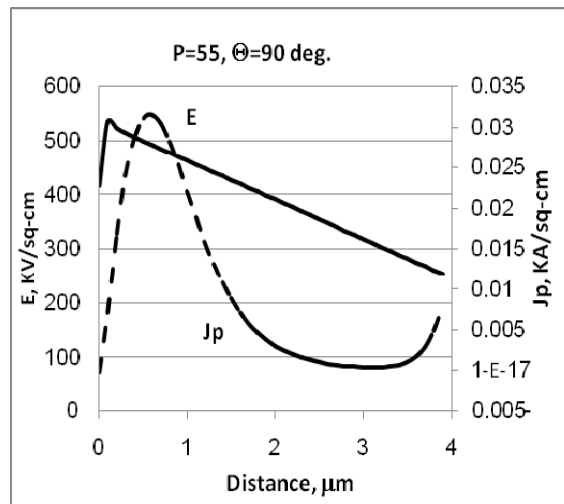


Fig. 9b:

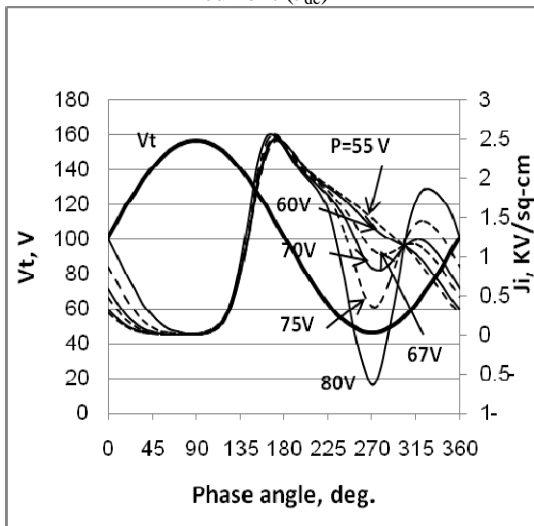


Fig. 8: The induced current (J_i) and the terminal voltage (V_t) for the peak voltage ranging from 55 to 80V

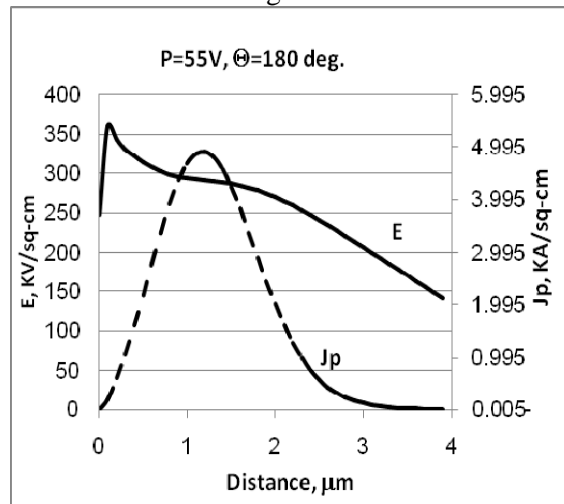


Fig. 9c

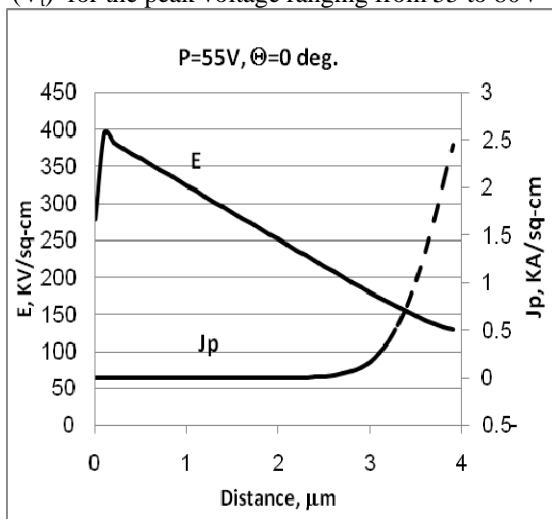


Fig. 9a:

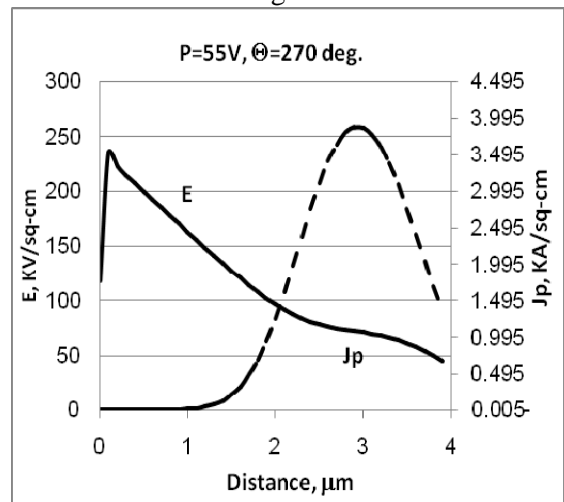


Fig. 9d:

Fig. 9: The spatial distribution of the electric field (E) and the hole current (J_p) for the peak voltage = 55 V at different values of phase angles

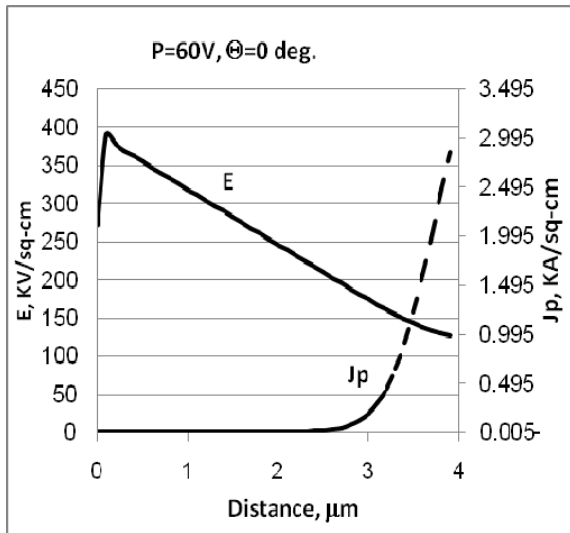


Fig. 10a

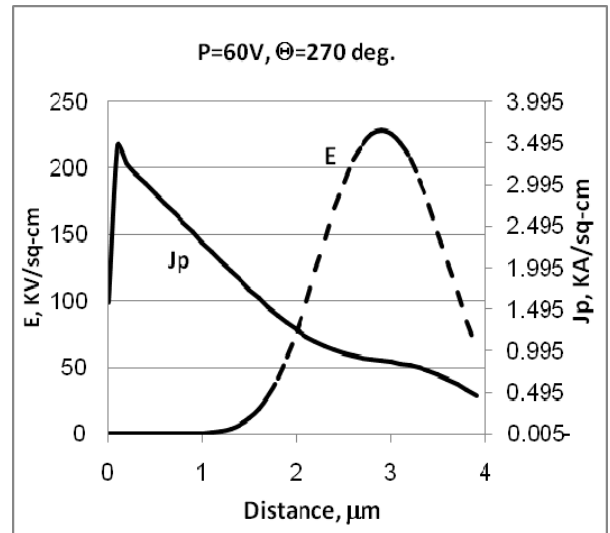


Fig. 10d:

Fig. 10: The spatial distribution of the electric field (E) and the hole current (J_p) for the peak voltage = 60 V at different values of phase angles

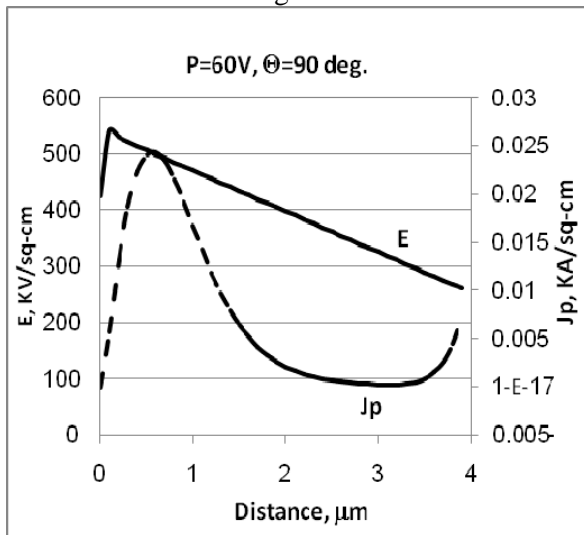


Fig.10b:

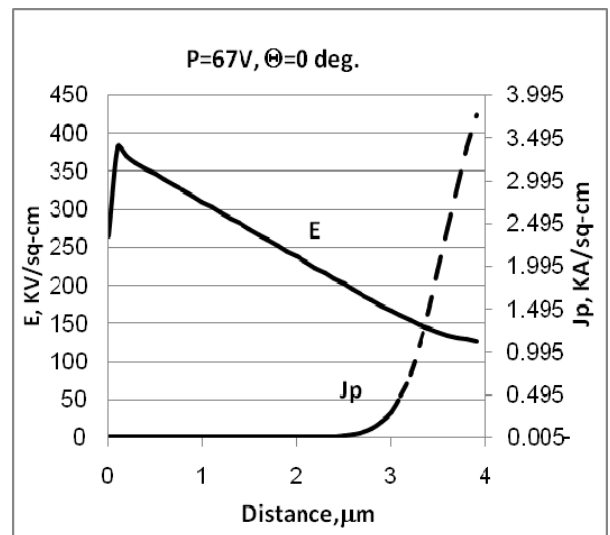


Fig. 11a:

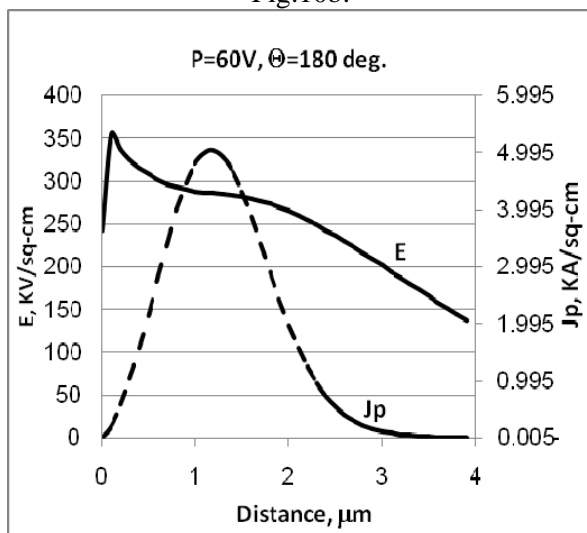


Fig. 10c

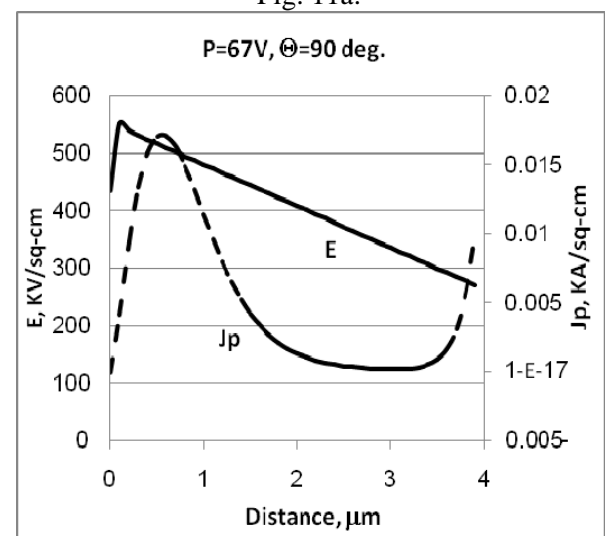


Fig. 11b:

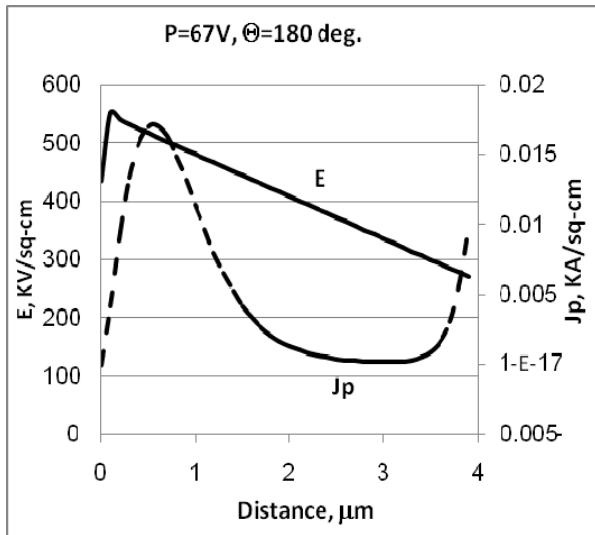


Fig. 11c:

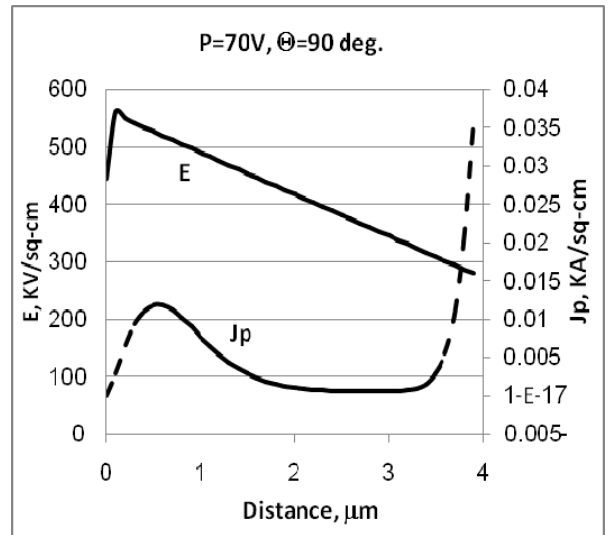


Fig. 12b:

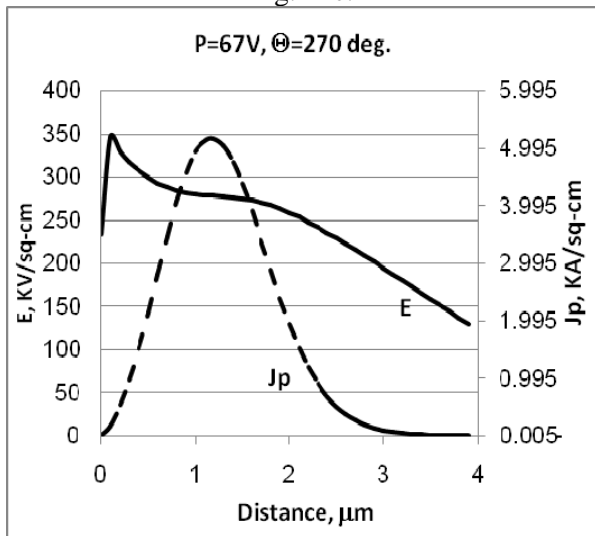


Fig. 11d:

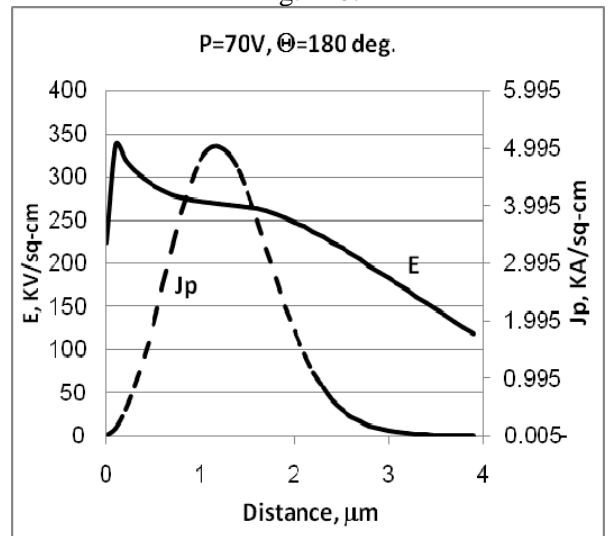


Fig. 12c

Fig. 11: The spatial distribution of the electric field (E) and the hole current (J_p) for the peak voltage = 67 V at different values of phase angles

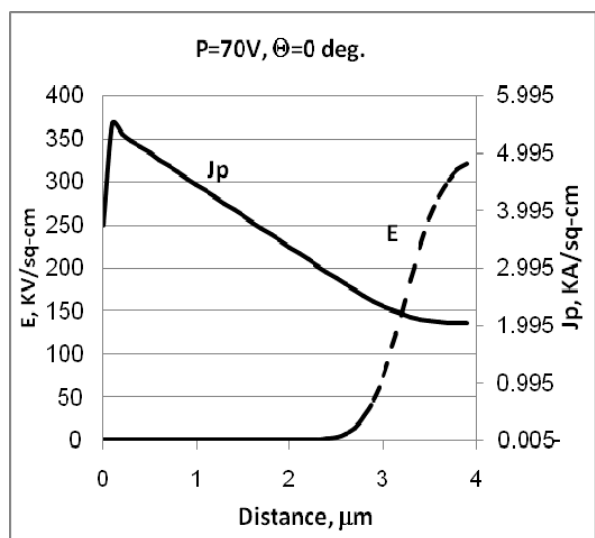


Fig. 12a:

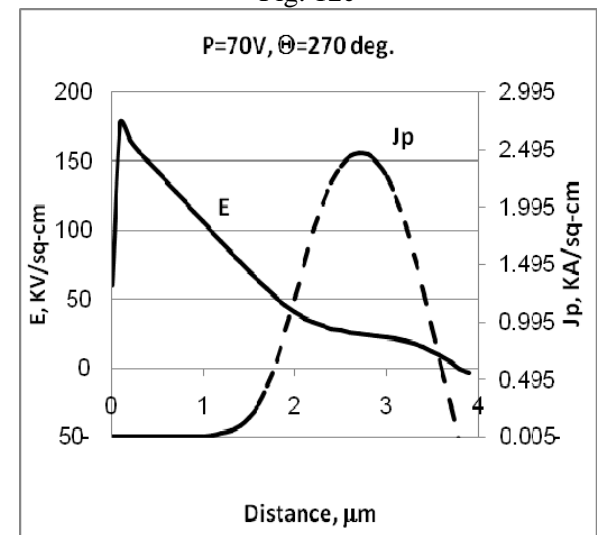


Fig. 12d

Fig. 12: The spatial distribution of the electric field (E) and the hole current (J_p) for the peak voltage = 70 V at different values of phase angles

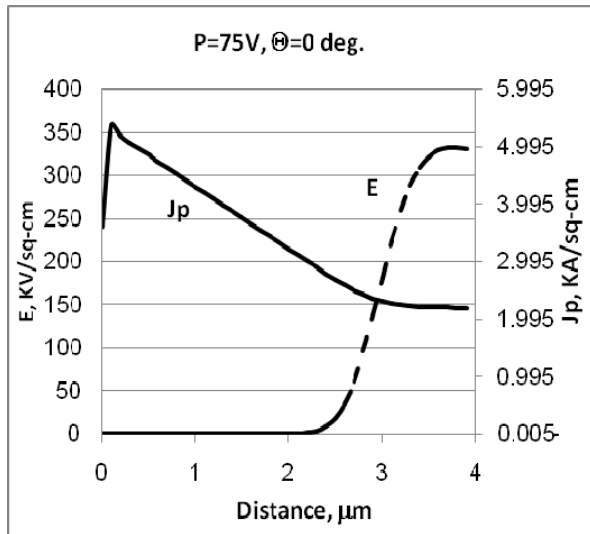


Fig. 13a:

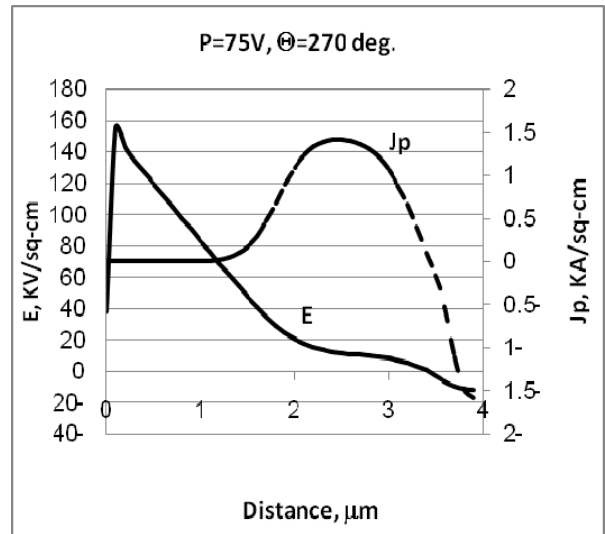


Fig. 13d

Fig. 13: The spatial distribution of the electric field (E) and the hole current (J_p) for the peak voltage = 75 V at different values of phase angles

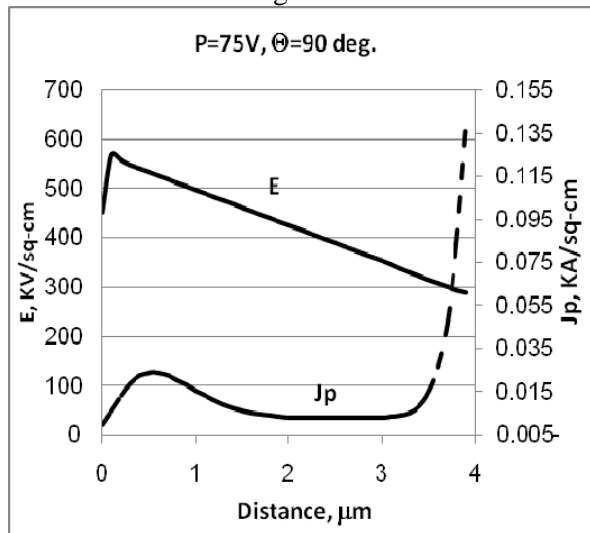


Fig. 13b

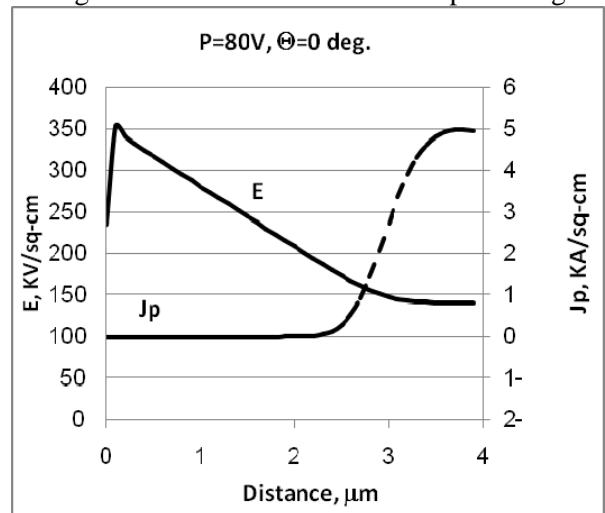


Fig. 14a

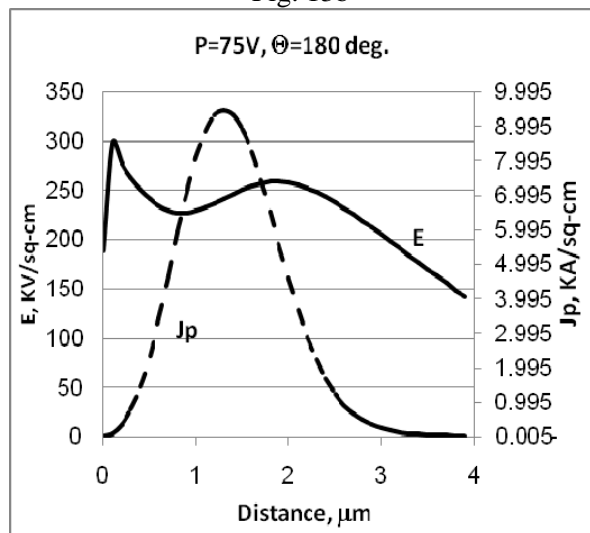


Fig. 13c

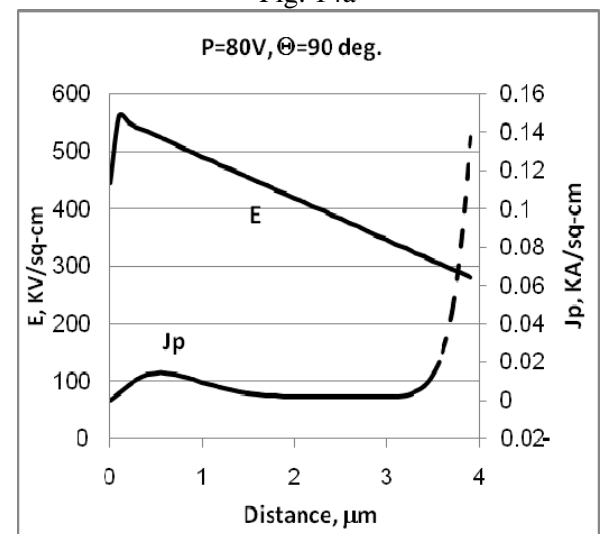


Fig. 14b:

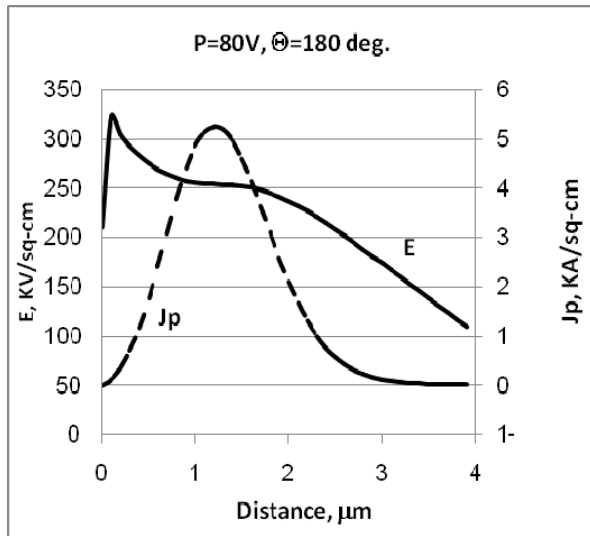


Fig. 14c

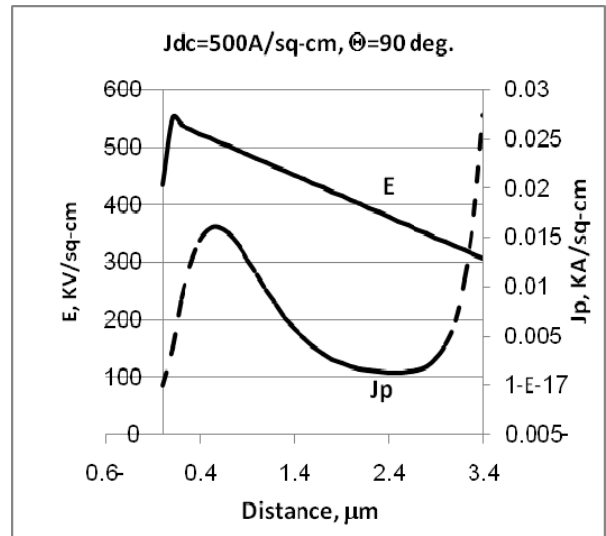


Fig. 15b:

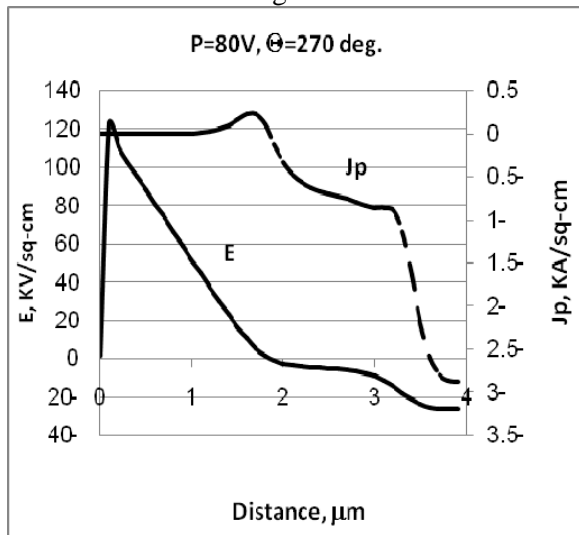


Fig. 14d

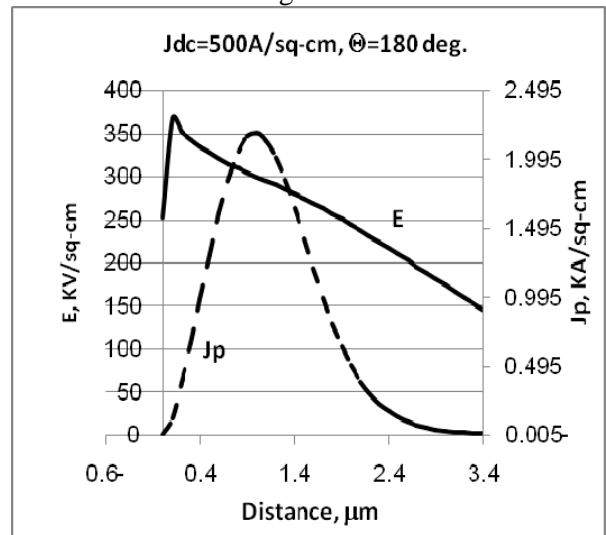


Fig. 15c

Fig. 14: The spatial distribution of the electric field (E) and the hole current (J_p) for the peak voltage = 80 V at different values of phase angles

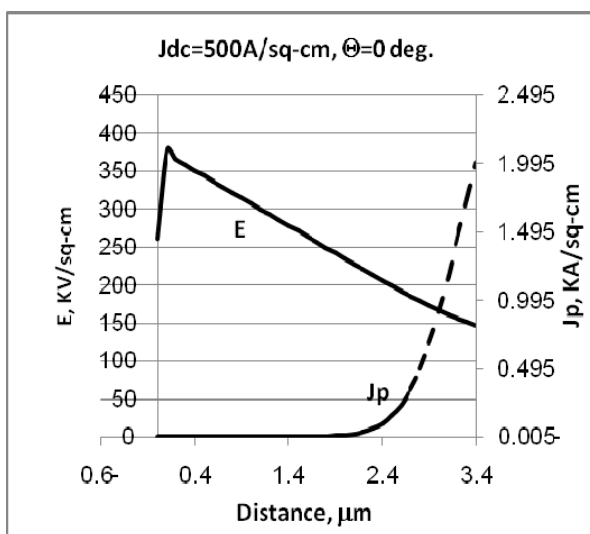


Fig. 15a:

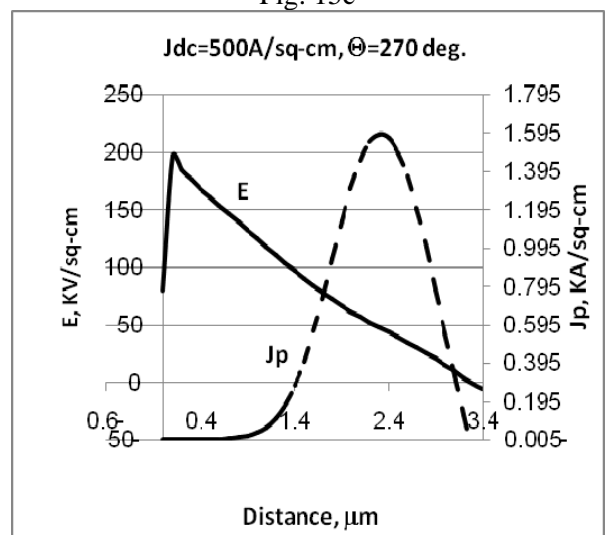


Fig. 15d:

Fig. 15: The spatial distribution of the hole current (J_p) and the electric field (E) at $J_{dc} = 500 \text{ A/cm}^2$ for different phase angles

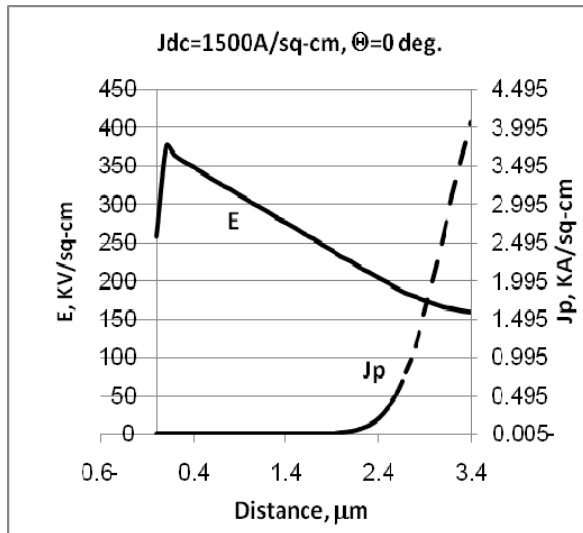


Fig. 16a:

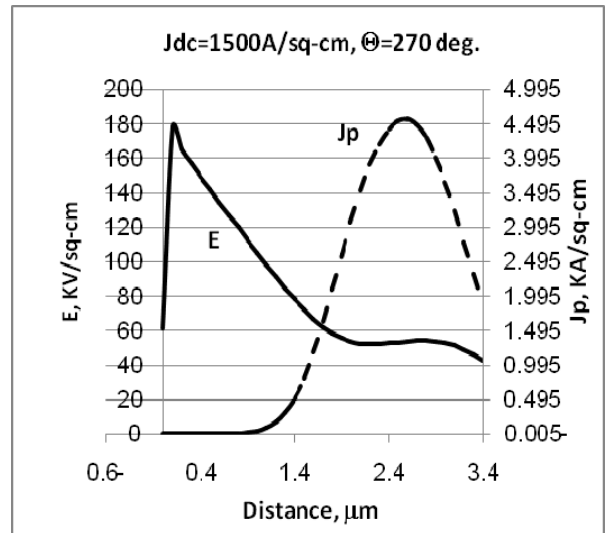


Fig. 16d:

Fig. 16: The spatial distribution of the hole current (J_p) and the electric field (E) at $J_{dc} = 1500 \text{ A/cm}^2$ for different phase angles

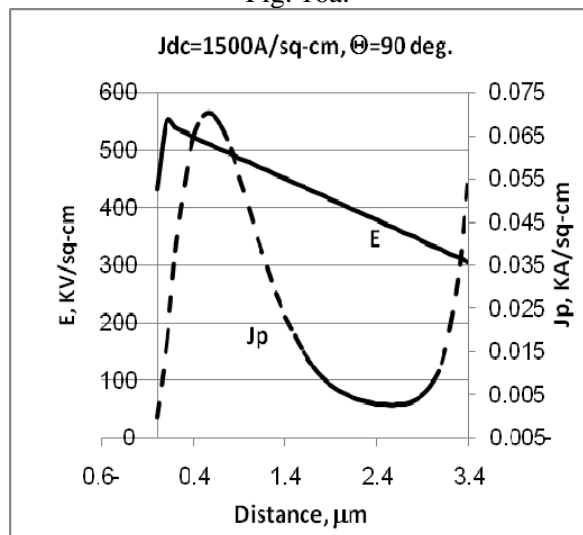


Fig. 16b:

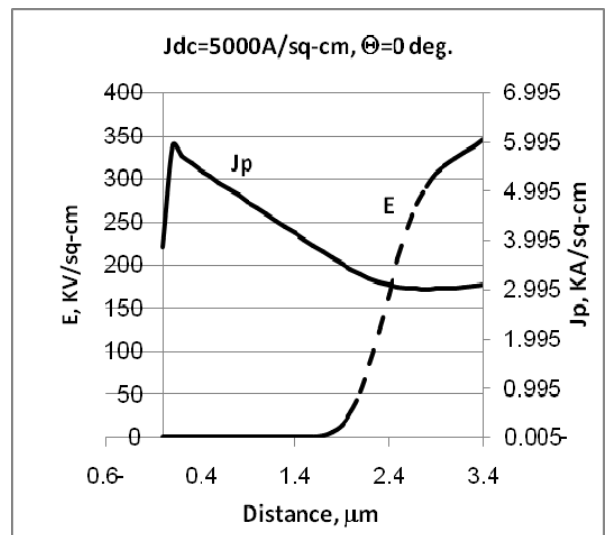


Fig. 17a:

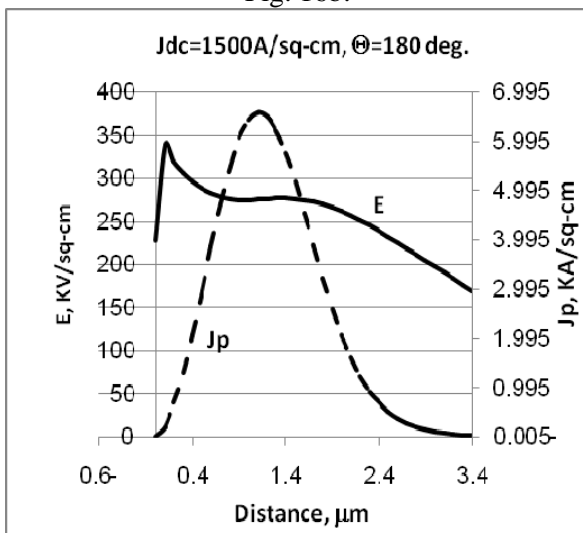


Fig. 16c

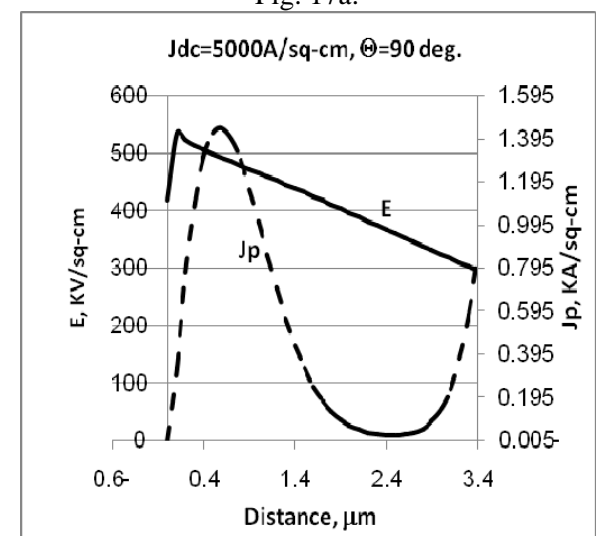


Fig. 17b:

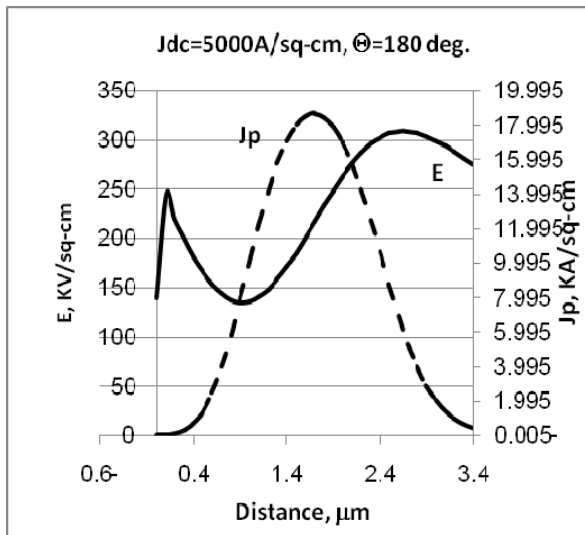


Fig. 17c

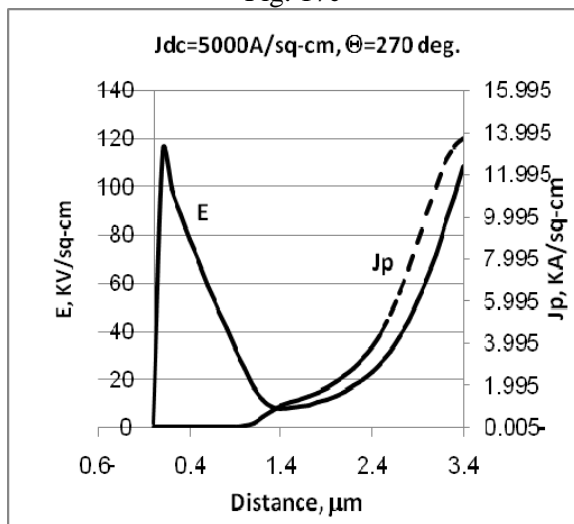


Fig. 17d:

Fig. 17: The spatial distribution of the hole current (J_p) and the electric field (E) at $J_{dc} = 5000 \text{ A/cm}^2$ for different phase angles

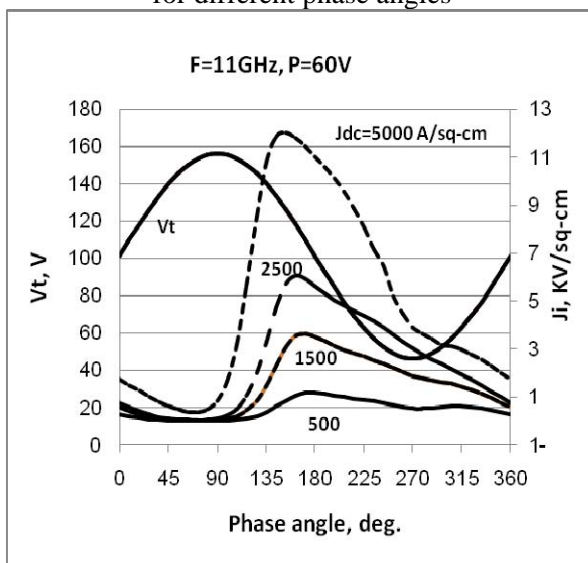


Fig. 18: The induced current (J_i) and the terminal voltage, (V_t) for dc current (J_{dc}) values ranging from 500 to 5000 A/cm^2

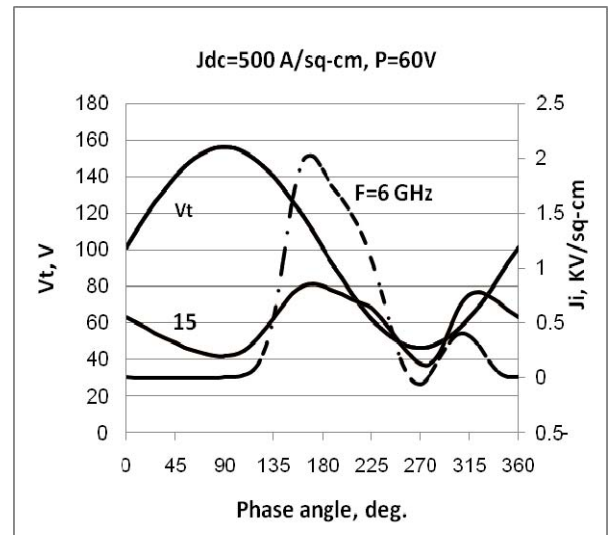


Fig. 19: The induced current (J_i) and the terminal voltage (V_t) for different values of the frequency (F)

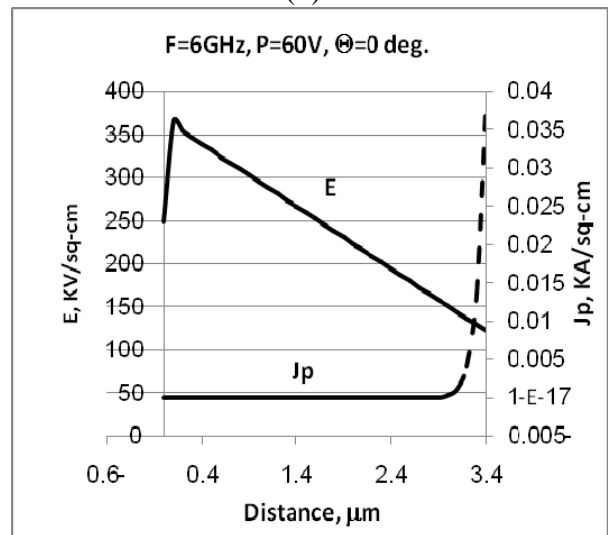


Fig. 20a

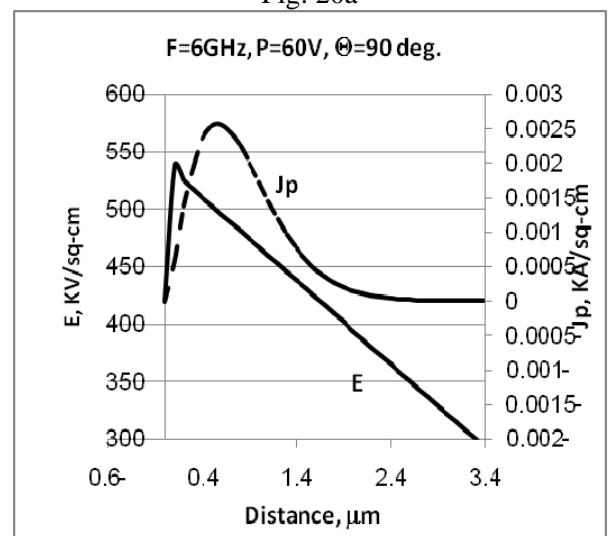


Fig. 20b

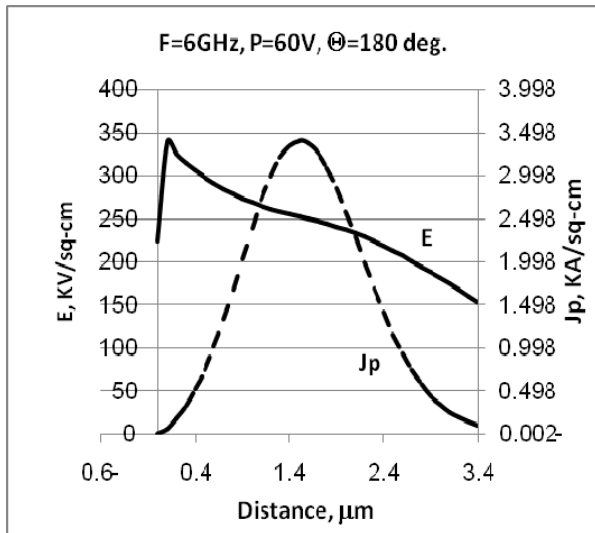


Fig. 20c

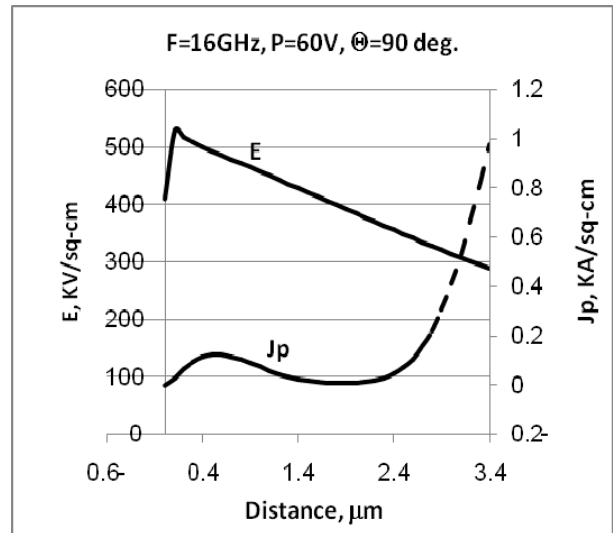


Fig. 21b:

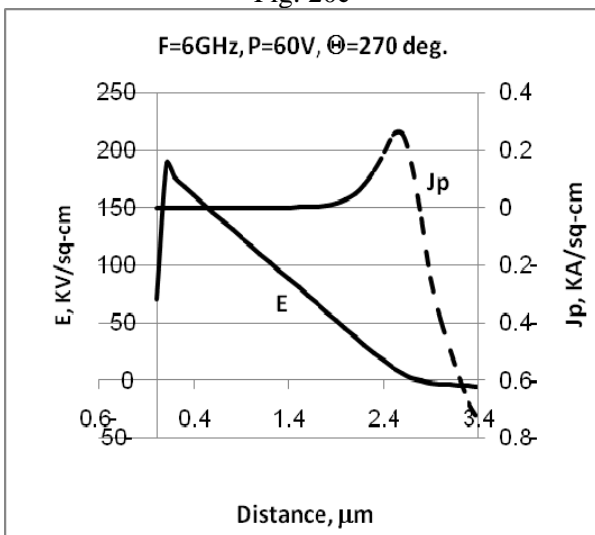


Fig. 20d

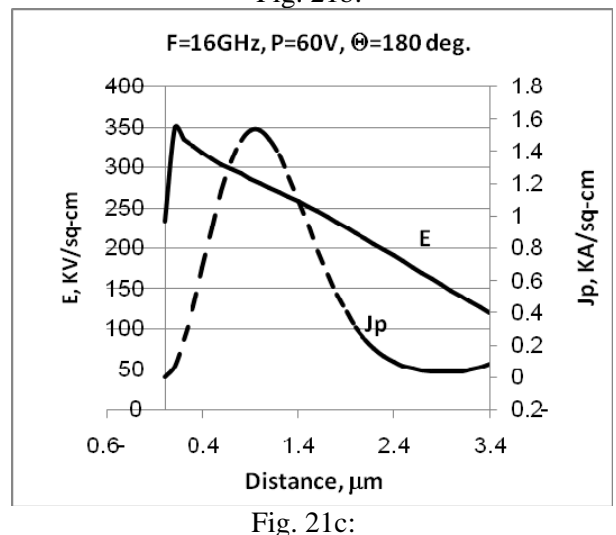


Fig. 21c:

Fig. 20: The spatial distribution of the hole current (J_p) and the electric field (E) at F= 6 GHz for different phase angles

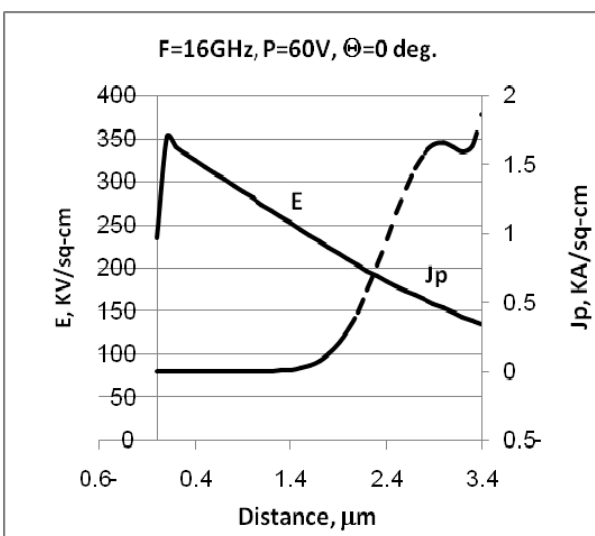


Fig. 21a:

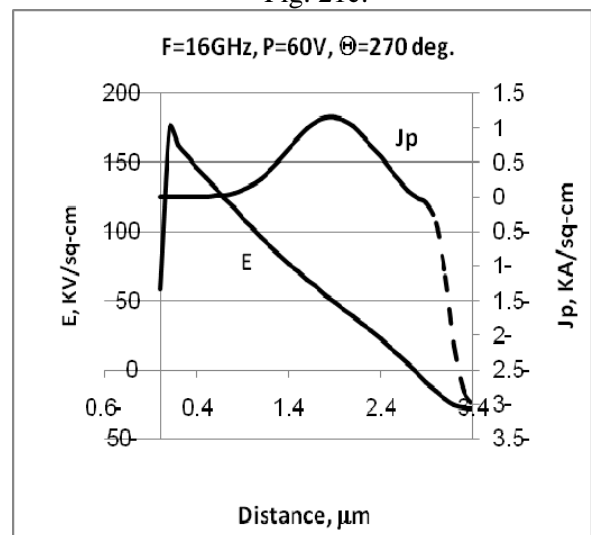


Fig. 21d:

Fig. 21: The spatial distribution of the hole current (J_p) and the electric field (E) at F= 16 GHz for different phase angles